Atmos. Meas. Tech., 7, 3653–3666, 2014
www.atmos-meas-tech.net/7/3653/2014/
doi:10.5194/amt-7-3653-2014

Atmospheric Measurement Techniques
Open Access

Rapid, optical measurement of the atmospheric pressure on a fast research aircraft using open-path TDLAS

B. Buchholz[1,2], **A. Afchine**[3], **and V. Ebert**[1,2]

[1]Physikalisch-Technische Bundesanstalt Braunschweig, Braunschweig, Germany
[2]Center of Smart Interfaces, Technische Universität Darmstadt, Darmstadt, Germany
[3]Forschungszentrum Jülich, IEK-7, Jülich, Germany

Correspondence to: V. Ebert (volker.ebert@ptb.de)

Received: 17 March 2014 – Published in Atmos. Meas. Tech. Discuss.: 13 May 2014
Revised: 19 August 2014 – Accepted: 8 September 2014 – Published: 6 November 2014

Abstract. Because of the high travel speed, the complex flow dynamics around an aircraft, and the complex dependency of the fluid dynamics on numerous airborne parameters, it is quite difficult to obtain accurate pressure values at a specific instrument location of an aircraft's fuselage. Complex simulations using computational fluid dynamics (CFD) models can in theory computationally "transfer" pressure values from one location to another. However, for long flight patterns, this process is inconvenient and cumbersome. Furthermore, these CFD transfer models require a local experimental validation, which is rarely available.

In this paper, we describe an integrated approach for a spectroscopic, calibration-free, in-flight pressure determination in an open-path White cell on an aircraft fuselage using ambient, atmospheric water vapour as the "sensor species". The presented measurements are realised with the HAI (Hygrometer for Atmospheric Investigations) instrument, built for multiphase water detection via calibration-free TDLAS (tunable diode laser absorption spectroscopy). The pressure determination is based on raw data used for H_2O concentration measurement, but with a different post-flight evaluation method, and can therefore be conducted at deferred time intervals on any desired flight track.

The spectroscopic pressure is compared in-flight with the static ambient pressure of the aircraft avionic system and a micro-mechanical pressure sensor, located next to the open-path cell, over a pressure range from 150 to 800 hPa, and a water vapour concentration range of more than 3 orders of magnitude. The correlation between the micro-mechanical pressure sensor measurements and the spectroscopic pressure measurements shows an average deviation from linearity of only 0.14 % and a small offset of 9.5 hPa. For the spectroscopic pressure evaluation we derive measurement uncertainties under laboratory conditions of 3.2 and 5.1 % during in-flight operation on the HALO airplane. Under certain flight conditions we quantified, for the first time, stalling-induced, dynamic pressure deviations of up to 30 % (at 200 hPa) between the avionic sensor and the optical and mechanical pressure sensors integrated in HAI. Such severe local pressure deviations from the typically used avionic pressure are important to take into account for other airborne sensors employed on such fast flying platforms as the HALO aircraft.

1 Introduction

Open-path tunable diode laser absorption spectroscopy (OP-TDLAS) is a promising approach for airborne in situ gas analysis. OP-TDLAS does not require a gas sample to be taken in a closed measurement cell. Instead, the gas is optically interrogated at its "natural" location (i.e. in situ) in an open, atmospheric light path. This has the advantage of circumventing typical sampling problems like chemical reactions in the sampling line, delay and integration effects due to the gas transport, or sampling artefacts related to wall adsorption in the piping. This is particularly critical for strongly adsorbing gases like ammonia, HCl or water vapour. OP-TDLAS in airborne scenarios thus allows measurements to be conducted directly outside the aircraft's fuselage, e.g. using open-path cells such as those described in Zondlo et al. (2010) and May (1998) or at least by having a large part of the optical path outside the airplane's boundary

layer (Diskin et al., 2002). Hence, OP-TDLAS is well suited for chemical analysis of reactive or strongly adsorbing gases like H_2O. However, absolute chemical species measurements – for example using TDLAS – also need accurate measurements of the physico-chemical boundary conditions, e.g. parameters like gas temperature and gas pressure. This is particularly true for airborne open-path gas analysis, and especially for calibration-free TDLAS techniques (Ebert and Wolfrum, 2000; Schulz et al., 2007), where, for example, no calibration to the flight speed is done and therefore pressure and temperature information is indispensable.

Pressure measurements represent a challenge in several ways, since they are needed for the final step in the evaluation of a volume concentration measurement (often applying the ideal gas law). The pressure might also be needed for the precalculation of fit parameters (like the collisional line width), thereby allowing a more robust fitting evaluation or a fit stabilisation during rapid concentration changes.

In principle, on an aircraft and in particular on a research aircraft such as the HALO (High Altitude and LOng Range) research aircraft (Krautstrunk and Giez, 2012), a good static ambient pressure calculation based on several sensors is available (Giez, 2012). But the related measurements are conducted in front of the nose of the aircraft (in a so-called "nose boom") and thus far away from most other sampling locations such as sampling inlets or our open-path cell, which could not be placed in an exposed spot like the nose boom. Through extensive computational fluid dynamics (CFD) models, each measured pressure value can be theoretically "converted" to any another location on the aircraft's fuselage. This, however, requires that all static dimensions of the airplane as well as dynamic flight and ambient air parameters be known or able to be measured. But, in practice, problems arise because an accurate CFD model of a newly developed aircraft is often the intellectual property of its manufacturer and thus not available for transfer calculations. Further, it is typically optimised to airplane development issues and not towards research issues. Consequently, the users need to set up their own CFD models, which is extremely time-consuming and often still inaccurate due to missing special data. These computationally intensive simulations for pressure transfer calculations then have to be made for all flight conditions, which again increases the work effort and computational load and thus calls for alternative ways to derive a local pressure, e.g. at the location of an airborne sensor outside the airplane.

In practice it is certainly a possibility to install a compact pressure transmitter directly at the measurement location. But this then leads to the need to validate the local pressure sensor and to compare it with the static pressure derived from the nose boom. An additional sensor outside the aircraft fuselage also requires substantial certification efforts, even for bird-strike certification tests and the like. Developing a special, certifiable pressure sensor interface could also result in an ambiguity and the need to determine the "real" pressure values and to compare it, for example, with the optical light path of the open-path cell. In an ideal case, pressure measurements need to be validated against multiple "reference" sensors, using an independent method parallel to the actual measurement.

Therefore, in this paper we describe, for the first time, an in-flight, open-path pressure determination method using calibration-free TDLAS with the challenge of performing the pressure measurement at the same time as the concentration measurement on the same, highly variable target measurand. These optical pressure measurements are subsequently used for the validation of a small, micro-mechanical pressure sensor installed close to the open-path TDLAS pressure measurement. In our case the target species is water vapour, despite its very large atmospheric concentration range and the aggravating in-flight conditions and the high gas velocity of about 900 $\mathrm{km\,h^{-1}}$.

2 Theory

2.1 Tunable diode laser absorption spectroscopy (TDLAS)

The setup and working principle of a typical TDLAS instrument is described in detail in many books, lecture notes and papers (e.g. Werle, 1998; Lackner, 2011; Schiff et al., 1994). The use of the dTDLAS (*direct* TDLAS) evaluation method for gas analysis, the aim of which is to avoid typical calibration procedures with reference gas standards containing a defined target gas mixture, is less common (Ebert and Wolfrum, 2000; Schulz et al., 2007; Farooq et al., 2008; Mihalcea et al., 1997). Numerous applications provide specific boundary conditions that prevent or significantly complicate a well-controlled calibration process. Such application scenarios include the sampling-free in situ gas analysis in combustion or other reactive processes like power plants (Ebert et al., 2003) or the detection of gas species like NH_3 (Pogány et al., 2010) where the preparation, storage and transport of calibration gas mixtures is complicated or even currently impossible. In such situations, where mobile calibration sources are difficult to obtain (such as for water vapour at low (< 100 ppmv) mixture fractions), the benefits of calibration-free sensing principles can be fully utilised. Nevertheless, a calibration-free instrument can also still be calibrated/validated, e.g. after a campaign (Buchholz et al., 2013b), so it is not a choice for or against a principle.

The principle of non-calibrated, absolute dTDLAS is presented here very briefly (in reference to the above-mentioned literature), and the bulk of the effort is focused on the extraction of pressure values from the dTDLAS raw signals intended for species concentration measurements.

2.2 Non-calibrated, direct TDLAS (dTDLAS)

2.2.1 Basic setup

The instrument (called "HAI" – Hygrometer for Atmospheric Investigations) used in this paper to extract absolute, high-speed pressure measurements from an open-path absorption signal is designed first and foremost for open-path water vapour concentration measurements aboard a specialised high-speed research aircraft (HALO: see www.halo.dlr.de), but the major functions for determining water vapour concentrations are secondarily for pressure measurement. In the interest of a detailed description of the pressure measurement principles we refrain from explaining all details of the concentration detection procedure, the basic details of which have also been explained in detail elsewhere.

The basic setup of the HAI spectrometer is shown in Fig. 1 and can be visualised in two separate building blocks. Block a is the actual open-path measurement setup (Fig. 1, left) where the water molecules are detected. The entire data evaluation of the spectrometer is concentrated in building block b, which comprises the main electronics unit of the spectrometer (Fig. 1, right). This spatial separation of the two building blocks allows the spectrometer optics to be adapted to the specific requirements of the individual application and is often advantageous when conditions at the measurement region itself are complex or critical (such as open-path measurements on the outer skin of an aircraft). Therefore the open-path cell of the HAI hygrometer has a direct fibre coupling without any transfer optics and a built-in detector. This avoids exposing the rest of the spectrometer components to the large temperature (−70 to +50 °C) and pressure (1000–150 hPa) fluctuations by installing them in the aircraft cabin.

An absolute evaluation of dTDLAS raw signals to yield mixture fractions of the target species, which is possible with an accuracy in the single-digit percentage range (Buchholz et al., 2014) for H_2O concentrations, requires absolute gas temperature and gas pressure measurements inside the open-path cell. The temperature data needed for the laser signal evaluation are typically measured by a local temperature T sensor at or near the open-path section. The pressure within the measurement region is usually derived from a pressure transmitter whose interface is located inside the optical unit of building block A and which senses the gas pressure. This is reliably done via a pressure pipe, as long as the frequency of the pressure variations over the flow time along the pipe length is negligible. In complex situations, like on high-speed airborne platforms, both values may be difficult to acquire due to dynamic effects. Therefore the open-path sensor has two temperature sensors and a built-in pressure sensor (described later) to provide, in combination with CFD models and several validations, reliable gas temperature and gas pressure values for the evaluation process.

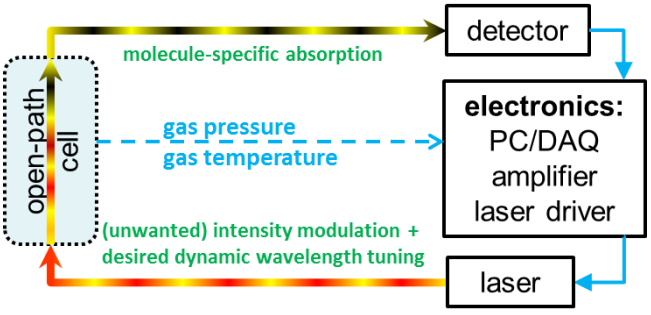

Figure 1. TDLAS principle and basic setup: the laser current modulation at typically 100 Hz–10 kHz initiates a rapid wavelength tuning in combination with a strong intensity modulation of the diode laser radiation. The molecule-specific light loss caused by the absorbers within the open-path cell is captured for each individual wavelength scan by a photodetector, digitised, and saved as raw data for subsequent data analysis.

2.2.2 Evaluation

One of the major steps of TDLAS spectroscopy is laser current modulation, which is derived from a frequency generator signal, which is used to control a laser current driver. The laser chip temperature is stabilised using Peltier elements driven by a separate temperature control loop. The laser current modulation frequency is typically chosen in the range of 100 Hz–10 kHz, with a typical laser dependent current amplitude of 1–150 mA. The current modulation induces the desired, continuous, dynamic wavelength tuning (typically $< 3\,\mathrm{cm}^{-1}$ for a distributed feedback laser (DFB) laser), as well as laser intensity modulation. After transmitting the laser light through the measurement region, the molecule-specific attenuation is captured and converted into a photocurrent using a detector, acquired with suitable data acquisition electronics, and saved to disk as raw data for further offline evaluation. In principle the HAI instrument contains two independent TDLAS spectrometers (working at 1.4 and 2.6 µm, respectively). For the spectroscopic pressure determination in this paper, solely the 1.4 µm part with the H_2O transition (000–101, 110–211) at 1370 nm ($7299.4\,\mathrm{cm}^{-1}$) is used.

The major evaluation steps to obtain the H_2O absorber concentrations are as follows: the wavelength-dependent light intensity $I(\lambda)$ captured behind the measurement region of thickness L is described via the extended Lambert–Beer equation (Eq. 1), which can be written as

$$I(\lambda) = E(t) + I_0(\lambda) \cdot \mathrm{Tr}(t) \cdot \exp\left[-S(T) \cdot g(\lambda - \lambda_0) \cdot N \cdot L\right], \quad (1)$$

with N being the number density of the molecular absorbers. The initial laser intensity $I(\lambda)$, the background emission $E(t)$ and the broadband transmission losses $\mathrm{Tr}(t)$ are synchronously derived from the individual raw signals and absorption profiles. Molecular line data like absorption line strength $S(T)$ and its temperature dependence are either

obtained from the HITRAN08 database (Rothman et al., 2009) or derived from our own dedicated measurements (Hunsmann et al., 2006). Other molecular spectral parameters, e.g. self- or foreign-broadening coefficients and their temperature dependence, as well as pressure-induced line shift, etc., of the normalised shape function $g(\lambda - \lambda_0)$ (centred at the wavelength λ_0) are also obtained from the same data sources.

The combination of the extended Lambert–Beer equation (Eq. 1) with the ideal gas law allows the amount fraction c to be derived:

$$c = -\frac{k_B \cdot T}{S(T) \cdot L \cdot p} \int \ln\left(\frac{I(\nu) - E(t)}{I_0(\nu) \cdot \mathrm{Tr}(t)}\right) \frac{\mathrm{d}\nu}{\mathrm{d}t} \mathrm{d}t. \quad (2)$$

In metrological units, the *amount fraction* c is correctly specified as [mol mol^{-1}: mol absorber per mol gas], which is more frequently assigned as "volume fraction" in the environmental community, e.g. in units of ppmv or vol%. In Eq. (2) the dynamic tuning coefficient of the laser $\frac{\mathrm{d}\nu}{\mathrm{d}t}$ (which is a constant property of the individual laser) and fundamental physical constants such as the Boltzmann constant k_B are needed to solve this equation. The first is derived experimentally using the airy signal of the laser light passing through a planar, air-spaced etalon (Ebert and Wolfrum, 2000; Schlosser et al., 2002). From long-term $\frac{\mathrm{d}\nu}{\mathrm{d}t}$ measurements over several years, we could verify, for the laser type used, a long-term stability of this basic laser property to better than 1 %, which is within the current uncertainties of the tuning characterisation.

For the pressure (p) and temperature (T) measurements it is important to note that no other hidden parameters generate unwanted additional degrees of freedom in the evaluation, and thus no calibration in particular has to be conducted for the target species. This explains why we term this technique "calibration-free". (Of course we have to calibrate our individual pressure and temperature sensors, but the response of the entire spectrometer with regard to the derived target gas concentration is not calibrated, in contrast to usual procedures; Muecke et al., 1994.)

2.3 Line broadening

The dTDLAS signal evaluation uses, via the spectral broadening parameters of the molecule, previous knowledge in order to model the precise shape of the molecular absorption signal contained in the raw signal. This modelling also connects the measured gas pressure and temperature with the spectral broadening parameters to the modelled line shape and line area. These links are therefore based on the dependence of the line shape, width and position of the absorption line used on changes in the physicochemical boundary conditions such as gas pressure and temperature, as well as composition of the gas matrix. As soon as sufficient information on the boundary conditions in the measurement zone is available, it is also possible to invert those relations and not only determine *absorber concentration* via laser absorption spectroscopy, i.e. dTDLAS, but also *gas temperature* (Teichert, 2003; Yang et al., 2011) or – as described here – also the *gas pressure*.

2.3.1 Line-broadening effects

The width of the absorption line, in our case the H_2O transition (000–101, 110–211) at 1370 nm (7299.4 cm^{-1}), is influenced by gas temperature, gas pressure and the matrix composition. For atmospheric applications, the matrix changes can be ignored in most cases as the basic air composition remains constant. Regarding the individual broadening contributions, natural, Doppler and collisional broadening have to be considered. Natural line broadening is too small to be noted in tropospheric signals and thus can be neglected at these conditions. The influence of temperature-induced broadening by the Doppler effect arises from the absorber movement because each molecule, depending on its velocity of movement towards the light, is penetrated in its inertial system by a small Doppler-shifted light frequency. Therefore, this velocity (and hence the frequency) is Maxwell–Boltzmann-distributed and can be described by a Gaussian shape function with the width $\gamma_{\mathrm{Doppler}}$ as follows:

$$\gamma_{\mathrm{Doppler}} = \left(\frac{\nu_0}{c}\right)\sqrt{\frac{2kT\ln 2}{m}} = 3.581 \times 10^{-7} \nu_0 \sqrt{\frac{T}{M}}. \quad (3)$$

If the gas temperature is measured in the experiment with sufficient accuracy, Doppler broadening can be calculated directly and thus does not have to be fitted.

The collisional broadening, which mainly describes the pressure influence, i.e. the interaction between the absorber molecule and its collision partners, is to be discerned with regard to collisions between absorber species (leading to *self*-broadening) or "mixed" absorber-matrix-species collisions (leading to *foreign* broadening). This process is also strongly affected by the complexity (Peach, 1981), type (long/short-range forces) and strength of the interaction and the quantum state of both collision partners. Collisional broadening coefficients thus typically have to be determined experimentally. The commonly used line shape profile is the Lorentzian shape function. The pressure and temperature dependence of the collisional half-width can be empirically expressed as

$$\gamma_{\mathrm{Lorentz}} = \left(\gamma^0_{\mathrm{L\,self}} \cdot p_{\mathrm{self}} + \gamma^0_{\mathrm{L\,foreign}} \cdot p_{\mathrm{foreign}}\right) \frac{1}{p_0} \left(\frac{T_0}{T}\right)^n. \quad (4)$$

The broadening coefficients γ ($\gamma^0_{\mathrm{L\,self}}$ representing self-broadening, and $\gamma^0_{\mathrm{L\,foreign}}$ foreign broadening) are obtained from databases such as HITRAN (Rothman et al., 2009) or from own measurements (Ortwein et al., 2010) when the database accuracy is inadequate or a certain foreign gas mixture coefficient is not available in the literature. p_{self} and p_{foreign} are the partial pressures of the target absorber gas (here water vapour) and the individual surrounding gas

species (here air as a gas mixture), respectively. The factor $\frac{1}{p_0}$ with $p_0 = 1\,\text{atm} = 1013.15\,\text{hPa}$ is used to scale the γ values to the common units $\text{cm}^{-1}\,\text{atm}^{-1}$.

The temperature dependence of the collisional broadening is specified by the temperature coefficient n and must be specifically considered when temperature-variable measurements, far away from the reference temperature $T_0 = 296\,\text{K}$, are conducted. Typical values for n are between 0.4 and 0.9. For the water line used in this paper we had previously determined n to be 0.74 (Hunsmann et al., 2006).

2.3.2 Superposition of broadening effects

The Doppler and collisional broadening mechanisms have to be convoluted to the so-called Voigt line shape to represent the measured absorption line shape profile. This Voigt profile cannot be expressed in purely analytical form. However, numerous numerical approximations are available in the literature, e.g. Herbert (1974), Armstrong (1967) Klim (1981). A commonly used approximation that takes relatively little calculation time can be written as (Olivero and Longbothum, 1977)

$$\gamma_{\text{voigt}} = 0.5346 \cdot \gamma_{\text{Lorentz}} + \sqrt{\left(0.2166\gamma^2_{\text{Lorentz}} + \gamma^2_{\text{doppler}}\right)}. \quad (5)$$

The Voigt approximation neglects higher-order effects such as Dicke narrowing (Dicke, 1953), for which higher-order line shape (HoLS) models such as Galatry (Galatry, 1961) or Rautian– obel'man (Rautian and Sobel'man, 1967) profiles are needed. HoLS models can be interesting at high signal-to-noise ratios (SNR) and lower pressure when $\gamma_{\text{Lorentz}} < \gamma_{\text{Doppler}}$ (Kochanov, 2000, 2011; Lepère, 2004; Pickett, 1980; Varghese and Hanson, 1984). The range at 1370 nm for the absorption line used is about 0.1–0.02 cm^{-1} for γ_{Lorentz} and 0.01 cm^{-1} for γ_{Doppler} in typical atmospheric conditions (200–1000 hPa). Strict minimisation of the degrees of freedom of the fit is an issue, in particular for low signal-to-noise spectra, which can strongly influence the fit stability and reliability. Thus, with respect to the objective to measure pressure (and concentration) on fast airborne platforms, we did not use HoLS since they would only be interesting for the lowest targeted atmospheric pressure range, where the SNR is, due to the associated low H_2O concentrations, also low.

2.4 Pressure determination using TDLAS

Many TDLAS studies on pressure broadening (e.g. Ortwein et al., 2010; Pustogov et al., 1994; Vorsa et al., 2005; Giesen et al., 1992) are available in the literature. These use in principle the inverse method for pressure determination via TDLAS (e.g. Brown et al., 2010).

Figure 2 shows – at constant temperature and humidity – the above-discussed Voigt line shape profiles for different pressures. The pressure-induced line broadening clearly offers the possibility to determine the total pressure from the

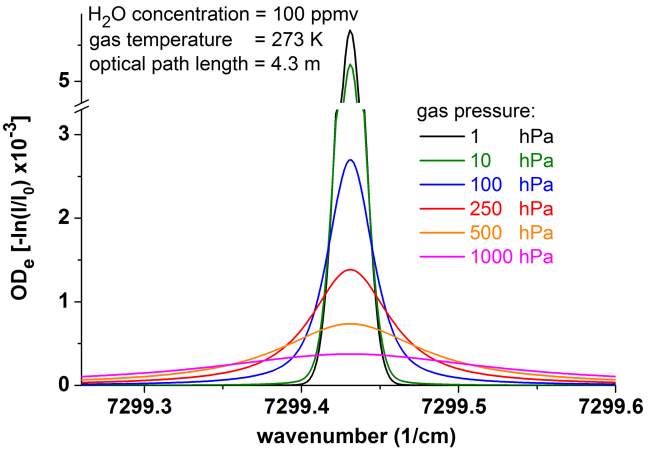

Figure 2. Simulated absorption profiles of the used (000–101, 110–211) water vapour transition at 1370 nm (7299.4 cm^{-1}) at 100 ppmv water vapour for the atmospheric pressure range between ground level and the mid-stratosphere. The line width is mainly influenced by the collisional, foreign broadening by air, inducing a Lorentzian line shape for gas pressures above 100 hPa. At the lowest pressures of 1 and 10 hPa the line shape (Gaussian) is mainly influenced by Doppler broadening.

measured line broadening. The apparent problem of the algebraically missing solution for the deconvoluted Voigt function can be solved by a precalculation of the Doppler component with the measured gas temperature as described in Eq. (3) and fitting the Voigt line shape to the measurement data by using the Voigt approximation (Eq. 5) to obtain the Lorentzian width γ_{Lorentz}.

The partial pressures in the equation for the Lorentzian width Eq. (4) can be replaced by the water concentration combined with the total gas pressure. Thereby, the total gas pressure p becomes separable (Eq. 6),

$$\gamma_{\text{Lorentz}} = \left(\gamma^0_{\text{L H}_2\text{O self}} \cdot C_{\text{H}_2\text{O}} + \gamma^0_{\text{L air foreign}} \cdot \left(1 - C_{\text{H}_2\text{O}}\right)\right) \cdot \frac{p}{p_0} \cdot \left(\frac{T_0}{T}\right)^n, \quad (6)$$

and can thus be isolated (Eq. 7)

$$p = \frac{\gamma_{\text{Lorentz}} \cdot p_0}{\left(\gamma^0_{\text{L H}_2\text{O self}} \cdot C_{\text{H}_2\text{O}} + \gamma^0_{\text{L air foreign}} \cdot \left(1 - C_{\text{H}_2\text{O}}\right)\right) \cdot \left(\frac{T_0}{T}\right)^n}. \quad (7)$$

Equation (7) contributes to the following discussion: (A) the Lorentzian width γ_{Lorentz} can be determined (as described above) using the fitting process during absorption profile evaluation. Again, the dynamic tuning coefficient of the laser $\frac{\text{d}\nu}{\text{d}t}$ is needed to transfer the raw scan from time space to wave number space. (B) The foreign-broadening coefficient ($\gamma_{\text{L air foreign}}$) and the self-broadening coefficients ($\gamma_{\text{L H}_2\text{O self}}$), are molecule-specific parameters and can be measured in an independent lab experiment, or taken from

HITRAN[13], but with relatively large uncertainties of 5 % and even 10 % for foreign and self-broadening, respectively. Since the foreign-broadening coefficient has a significantly larger influence we recently re-measured it with improved uncertainty (HWHM 0.1077 cm atm^{-1} ±2.5 %) at the PTB (Physikalisch-Technische Bundesanstalt) national humidity standard (Heinonen, 2002). (C) The influence of the concentration C_{H_2O} on the optical pressure measurement has to be critically discussed, because conversely, for calibration-free concentration evaluation (Eq. 2), the absolute gas pressure is required. For typical atmospheric water vapour concentrations ranging from single-digit ppmv to approximately 45 000 ppmv (at −70 to +40 °C), the relative influence of self-broadening is strongly suppressed under most atmospheric sections (Fig. 3, left) and certainly well below 10 %. Figure 3 (right) shows for better visualisation a typical smoothed atmospheric water vapour profile. The pressure on the x axis is directly correlated to the flight height and, finally, with the altitude above the ground. Hence, even when the pressure is unknown, an iterative curve-fitting process can be done by neglecting the self-broadening ($C_{H_2O} = 0$) at the first iteration. Using this pressure value, the first calibration-free C_{H_2O} evaluation iteration can be executed in order to obtain the maximum 10 %-deviated C_{H_2O} values (Eq. 2). These values can be used in the second iteration to reduce the maximum total gas pressure deviation to 1 % by neglecting all other deviation contributions.

An alternative way which avoids the iterative process can be described as follows: Eq. (2) can be written as $p \cdot c_{H_2O} = \frac{k_B \cdot T}{S(T) \cdot L \cdot} \int \ln\left(\frac{I(\nu) - E(t)}{I_0(\nu) \cdot \mathrm{Tr}(t)}\right) \frac{\mathrm{d}\nu}{\mathrm{d}t} \mathrm{d}t$, where the line area $\int \ln\left(\frac{I(\nu) - E(t)}{I_0(\nu) \cdot \mathrm{Tr}(t)}\right) \frac{\mathrm{d}\nu}{\mathrm{d}t} \mathrm{d}t$ can be evaluated directly from the fitting process.

Equation (6) can thus be rewritten as

$$p = \frac{\gamma^0_{\mathrm{Lorentz}} \cdot p_0 \cdot \left(\frac{T}{T_0}\right)^n - (\gamma^0_{\mathrm{L\ H_2O\ self}} + \gamma_{\mathrm{L\ air\ foreign}}) \cdot p \cdot C_{H_2O}}{\gamma^0_{\mathrm{L\ air\ foreign}}}.$$

From a practical point of view the fitting process can be better controlled and monitored in the iterative procedure, since the fitting process of noisier absorption profiles from field situations is less robust as it also has to correct for various optical disturbances.

Combining all broadening influences and applying them to typical atmospheric conditions (described by pressure, temperature and concentration profiles vs. height), the simulated profiles shown in Fig. 4 for the four selected height levels (marked “1” to “4” in Figs. 3 and 4) can be obtained. The individual pressure, temperature and self-broadening contributions to the line width are graphically illustrated in Fig. 5 for a mid-value and two extremes, which show the maximum range of the contribution that can be found under typical atmospheric variations. These contributions are considered later in detail when estimating the uncertainty contributions to the optical pressure determination.

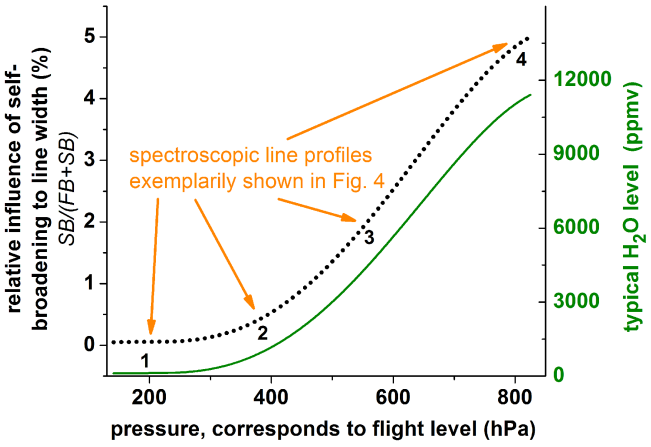

Figure 3. Typical atmospheric vertical water vapour concentration profile (green solid line) vs. total pressure. The total pressure is usually the preferred indicator for flight height. Also shown (black broken line) is the height dependence of the relative contribution (in percent) of self-broadening to the total line width for the water transition used (1370 nm). This shows that self-broadening correction is absolutely essential for precise spectroscopic pressure measurement as the self-broadening can contribute up to 5 % to the total width. Four selected absorption profiles at different flight levels indicated by numbers 1 to 4 are depicted in Fig. 4.

Crucial in this process and similar to calibration-free concentration evaluation (Sect. 2.2) is the design of the optical pressure determination procedure in a way that avoids any pressure calibration for the optical signal. An accurate pressure calibration at 900 km h^{-1} air speed would indeed be quite difficult to achieve, especially because a calibration under static conditions is very difficult to transfer to the highly dynamic, high-speed flow situation on a flying aircraft. The calibration-free optical pressure determination is therefore an elegant method to provide an independent way of validating other built-in, classical, in-flight pressure sensors in the measurement region.

Generally it can be stated that water vapour is certainly a suboptimal sensor species for pressure determination owing to its very high atmospheric variability (more than 4 orders of magnitude) and its very low signal levels in and above the tropopause (compare Fig. 3). Other more suitable molecules like CO_2, CH_4 etc. show negligible self-broadening effects and much weaker changes in the SNR, e.g. the atmospheric CO_2 fluctuations are much smaller (only double-digit percentage range at a basis concentration of about 400 ppmv). However, the primary goal of the HAI open-path sensor (Buchholz et al., 2013a) is the realisation of a calibration-free, multi-phase water vapour measurement, for which the built-in micro-mechanical pressure transmitter has to be validated to stabilise and accelerate HAI’s fitting process. Thus an optical, water-based pressure determination is more an additional benefit of the HAI instrument which comes at very little extra cost but which

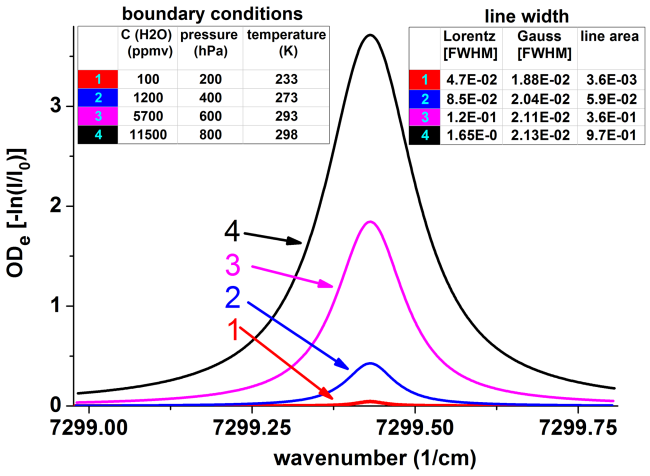

Figure 4. Simulated atmospheric H_2O absorption profiles at positions 1 to 4 in Fig. 3 illustrating the effect of (see text for details) temperature and foreign- and self-broadening on the used water transition (1370 nm) for a typical vertical atmospheric height profile. Parameter sets (T, p, C) of the individual lines and the resulting line widths are also shown. All line shapes are based on the same Voigt profile approximation, which is also used to pursue the fitting process.

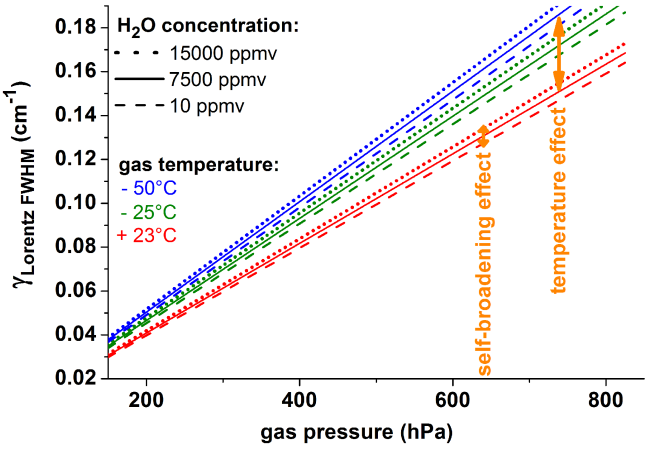

Figure 5. Collisional line widths $\gamma_{\mathrm{Lorentz}}$ induced by foreign broadening (of the used 1370 nm transition) as a function of flight height (scaled as total pressure) for three atmospheric temperatures (−50 °C, −25 °C, +25 °C), indicating the strong pressure and temperature dependence of the collisional width. In addition the influence of self-broadening on the line width is shown for high, medium and low H_2O concentrations (dashed lines). A clear hierarchy becomes visible with the largest impact from pressure, then temperature, then matrix composition. Thus the line width can be used for optical pressure determination if the latter two can be compensated for, i.e. if concentration (self-broadening) and temperature effects are corrected for.

significantly improves HAI's performance and robustness. With knowledge of the correct and validated total gas pressure, a spectrally stabilised spectrometer such as the HAI can precalculate pressure-dependent spectral parameters such as the pressure shift of the absorption line position, as well as the line broadening, and provide them as predetermined parameters, thereby significantly minimising the degrees of freedom and thus the stability and robustness, as well as the accuracy, of the spectral fitting process. Ultimately the degrees of freedom for the absorption line could be reduced to one final value, namely the line area. This procedure may be executed only when the pressure transmitter data adequately matches with the spectroscopically "sensed" pressure.

2.5 Uncertainty consideration

For measurements under harsh conditions and with complex flow dynamics (e.g. on the aircraft fuselage), it is difficult to assign a measurement uncertainty in the metrological sense (Joint Committee for Guides in Metrology (JCGM), 2008). Nevertheless, the uncertainty is estimated for the purpose of classifying the accuracy of the final measurands (and always stated as 1-sigma values).

First, the measurement by itself should be evaluated under laboratory conditions, followed by estimates of the additional influences when the measurements are performed on an aircraft. To estimate the total uncertainty of the "optical" pressure, which is determined via Eq. (7), we take into account the error in the self-broadening coefficient ($\gamma^0_{\mathrm{L\ H_2O\ self}}$), which is taken from the HITRAN08 database (Rothman et al., 2009) with 10 % uncertainty (1σ). The temperature coefficient (n) was measured by our group within 5 % (Hunsmann et al., 2006), and the air broadening coefficient ($\gamma_{\mathrm{L\ air\ foreign}}$) is obtained from unpublished measurements at the PTB with an uncertainty of 2.5 %.

For the uncertainty calculation we assume a water vapour mixture fraction of 2000 ppmv, which is determined with an uncertainty of 5 %, and a gas temperature of 273 K determined with 1 K uncertainty, which can realistically be achieved under quasi-static conditions. Finally, the collisional width ($\gamma_{\mathrm{Lorentz}}$) was set to 0.12 cm^{-1} FWHM (full width at half maximum; equivalent to 560 hPa) with an uncertainty of 2 %, which includes a conservative uncertainty estimate for the fitting process and the uncertainty of the dynamic tuning, which has to be measured to evaluate the laser signals. Under laboratory conditions, all these contributions result in a total uncertainty in the optical pressure determination of 3.2 %. The largest relative contribution to the total uncertainty is caused by the uncertainty of the air foreign-broadening coefficient (58 % relative), followed by the measurement of the collisional width $\gamma_{\mathrm{Lorentz}}$ (38 % relative).

To transfer this uncertainty estimate to the in-flight open-path measurements on the aircraft's fuselage, it is necessary to adapt the uncertainties of the measurands to the in-flight situation. The gas temperature uncertainty is then assumed to be 7 K, which is derived as a quite conservative estimate from a CFD simulation of the pressure and

temperature field within the open-path cell. The uncertainty for the width determination (γ_{Lorentz}) is doubled in light of the harsh environments in the high-speed flow plus broadband light scattering or radiative detector offsets caused by the sun. In total this results in an overall uncertainty of 5.1 % for the optical pressure determination, with the largest contribution coming from the width measurement γ_{Lorentz} (61 %) followed by the uncertainty of the air broadening coefficient (23 %) and the temperature measurement (14 %). This estimate is realistic for absorption profiles such as in Fig. 7 (discussed later in detail), where the SNR is quite high. Clearly, during flight tracks with very strong optical disturbances or in general at very low H_2O concentrations the width uncertainty increases owing to the reduction of the SNR.

3 Installing the open-path cell on HALO

The "HAI" multiphase hygrometer was successfully tested on the HALO research aircraft during the first scientific HALO mission in the second and third quarter of 2012. The aim of this science campaign, called TACTS (Transport and Composition in the UT/LMS), was to study the seasonality in the upper troposphere–lower stratosphere (Engel et al., 2013). Additionally, HAI was part of the scientific payload during the ESMVal (Earth System Model Validation) (Schlager, 2014) campaign.

The highest achievable flight level of the HALO aircraft determines the practically relevant pressure range for sensor validation, which is approximately 150 to 1000 hPa. The installation schematics (depicted in Fig. 6) show the open-path sensor after being installed on the HALO fuselage. The White-type (White, 1976) open-path cell has a mirror base distance of approximately 15 cm, which yields an optical path length of 4.2 m (indicated in red between the pylons (27 cm height) in Fig. 6). The main electronics part and the HAI lasers are housed in the cabin. The HAI control unit and the open-path cell are connected via glass fibres. The air temperature within the HAI open-path is measured via two platinum PT100 sensors. Certification requirements made it almost impossible to develop an isokinetic temperature sensor which protrudes into the gas flow. Hence, simulation models will be developed by the Forschungszentrum Jülich to estimate and correct the boundary layer effects acting on the surface-mounted PT100 sensors. The resulting temperature offsets (and corrections) are not as critical for the optical pressure measurement and hardly affect the pressure validation discussed in this paper in view of the uncertainty budgets mentioned above.

The Hai open-path sensor also includes its own pressure sensor based on a commercial piezo pressure transmitter (Newport Omega). This sensor is installed behind a rectangular (relative to gas flow) interface in the open-path cell. Furthermore there is a second pressure "signal" via HALO's static ambient avionics pressure (Giez, 2012) which is calculated based on a multidimensional pressure determination at the aircraft's nose boom (Giez, 2012). Thus there are in total three independent pressure values which can be compared: the optical TDLAS and the piezo sensor within HAI, and the HALO avionic system.

The high complexity of the HAI multiphase hygrometer does not allow for a comprehensive description in this paper. Therefore, only the components relevant to the spectroscopic pressure measurement have been explained (Fig. 1). A full-length description of the HAI instrument is planned and will also be focusing on multi-phase H_2O measurements.

4 Results

4.1 Signal evaluation

A typical TDLAS absorption signal profile after baseline, offset and transmission correction is shown in Fig. 7 (top) for a water vapour concentration of approximately 1900 ppm at a temperature of 1 °C and 440 hPa pressure. Here, the DFB laser is scanned over the H_2O transition with a repetition rate of 240 Hz. The detector signal after the absorption path in the open-path HAI cell is digitised at 480 kS s^{-1} with 14 bit resolution. Before further evaluation, 50 individual raw absorption profiles are pre-averaged resulting in an effective time resolution of 210 ms. This averaged signal is fitted to the above-described Voigt profile to obtain the effective collisional contribution γ_{Lorentz} of the total line width (Eq. 6), which is then used to determine the pressure, as described above. Figure 7 (bottom) shows the residual between measurement and model as determined by the fitting process. The typical Allan variance evaluation of system stability is not an easy task for HAI owing to the high H_2O concentration fluctuations in the flight data. Thus we determine optical performance data for the HAI open-path sensor from the global residual variance (1σ), which we define as the standard deviation of the residual over the entire fit range. The ratio between the global residual variance and the peak optical density (OD_{Peak}) results in an SNR of about 483. Assuming a linear relationship between OD_{Peak} and the water vapour concentration C_{H_2O}, this value can be used to estimate the sensor resolution $\frac{C_{H_2O}}{\text{SNR}}$ to 3.95 ppmv. To compare this value with other spectrometers, a time and path length normalisation can be deducted, which results in a normalised resolution $\sigma_{\text{norm }[H_2O]} = 7.6\,\text{ppmv}\,\text{m}\,\text{Hz}^{-1/2}$.

The presented line width evaluations are exclusively targeted on the determination of the pressure and not the gas concentration. Due to the large dynamic range of the water concentration the resolution would also strongly depend on flight height and thus is not easy to state in a single performance parameter. However, preliminary results of a concentration evaluation of the 1.4 µm open-path HAI signals yielded at flight levels with 300 ppmv water vapour to a precision of 1.3 ppmv (1σ) at 0.2 seconds response time,

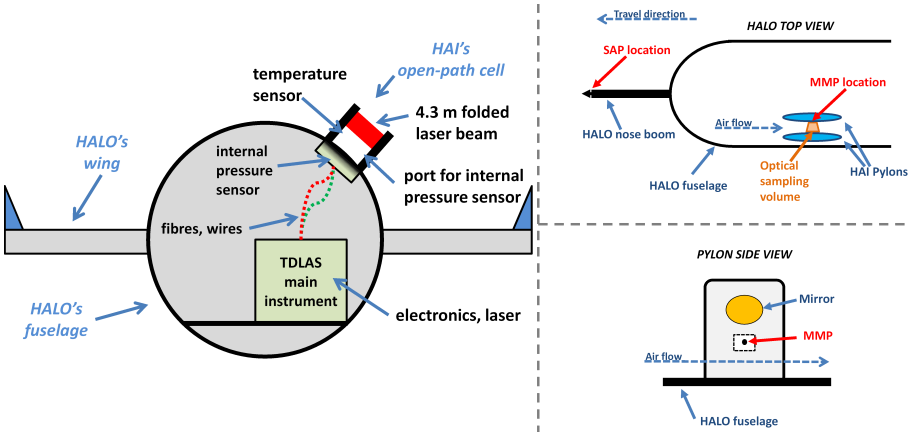

Figure 6. Schematics of the HAI open-path sensor installed on the HALO research aircraft fuselage. The open-path cell itself comprises two platinum PT100 sensors for air temperature measurements for use in data evaluation. Our HAI pressure measurement interface port allows for comparison between the "spectroscopically determined" pressure and a standard pressure transmitter (MMP). Additionally, several pressure sensors are installed in the nose boom of the HALO aircraft to measure the static ambient pressure (SAP).

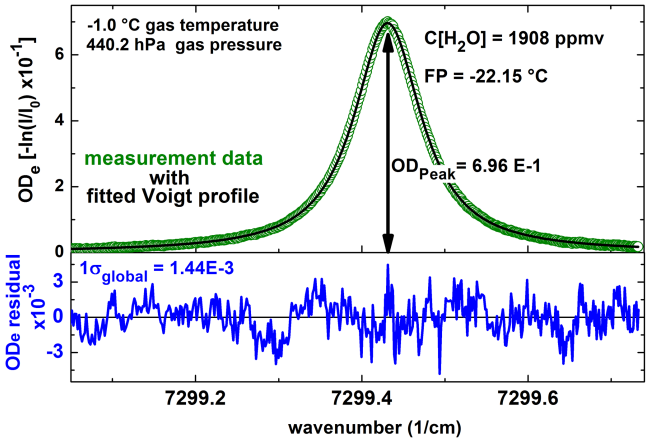

Figure 7. Typical, pre-processed, in-flight line profile measurement after baseline-, offset- and transmission correction. The DFB diode laser scans across the H_2O transition as shown with 240 Hz repetition rate; 50 individual raw scans are pre-averaged and the resulting average scan is then fitted, resulting in 210 ms time resolution. The global residual variance $1\sigma_{\text{global}}$ of the fit is defined as standard deviation of the residual over the shown entire fit range. It must be kept in mind that the gas flow is passing through the open-path cell at approximately 900 km h^{-1} (see text for more details).

determined via an Allan variance. These early evaluations also indicate a preliminary precision of 0.2 ppmv (1σ) for the 2.6 µm path under equal conditions.

4.2 In-flight intercomparison of pressure measurement techniques

Using the rare occasion of having available on an aircraft three independent pressure measurement techniques (a micro-mechanical pressure (MMP) transmitter, the static ambient avionic pressure (SAP) and the TDLAS pressure (TP)), we can realise an in-flight pressure sensor intercomparison under field conditions and discuss possible deviations between the individual sensors as well as a validation of the new, TDLAS-based, high-speed, optical pressure sensing technique.

When comparing these signals, however, one has to consider that the MMP and TP can be sensitive to local variations in the pressure field (both in a slightly different way) caused by the disturbance of the high-speed airflow in between the two HAI pylons. The local pressure variation will react strongly on the impact angle and speed of the airflow through the HAI cell and its dynamic variations, and thus obviously on the orientation of the HALO airplane relative to the major airflow. However, although this can be expected, until now it was not possible to directly detect and quantify such local pressure variations. Furthermore, since the avionic system does not have information on the local velocity field and fluid dynamics around HAI's open-path cell, it had to be expected that undetected local pressure modulation effects would modify the HAI water concentration in an unpredictable and an unquantified way when using the avionic data for evaluation of the HAI data. This was the main reason for developing an integrated, optical, open-path pressure monitoring system and comparing it with other means of dynamic pressure measurements.

In the following we compare the pressure signals in two typical situations: *disturbed* and *undisturbed*. Figure 8 shows a typical case of *undisturbed* superposition of the *three* pressure signals, captured during a descent of the HALO aircraft. This descent covers variations of a factor of 4 in pressure and a factor of 100 in H_2O concentration. The MMP transmitter (black line) is located (see rectangular pressure transmitter interface in Fig. 6) close to the optical

measurement volume defined by the open light path in the HAI White cell. The static ambient avionic pressure (SAP, red line) is derived from HALO's avionic system, measured at the nose boom in front of the airplane and directly processed via HALO's main data acquisition to provide the static ambient pressure. Finally, there is the spectroscopy-based TDLAS pressure (TP, blue line), which is discussed in this paper.

At first glance all three sensors pretty much coincide. Looking closer, the sensors show consistent and systematic discrepancies, with the SAP being always high, HAI's MMP always low (averaged difference SAP $-$ $-$MMP $= 28$ hPa) and the optical TP consistently in between. These deviations have a simple physical/fluid-dynamical explanation: since the air masses are accelerated in between the HAI pylons (see Fig. 6), they experience a dynamical pressure reduction relative to the ambient pressure, and thus MMP (black) and TP (blue), which are "sampling" between the pylons, have to be lower than the static ambient pressure (SAP, red) measured by the avionic system.

Comparing, furthermore, the two HAI pressure sensors, it has to be taken into account that the pressure measured directly by the MMP internal pressure transmitter in the open-path cell (black) must be lower, owing to the dynamic pressure reduction caused by the airflow parallel to the surface aperture of the MMP's pressure transmitter.

The obviously higher fluctuations of the TP are caused by a combination of several factors:

1. Real pressure fluctuations which cannot be detected by the slow and integrating MMP pressure transmitter.

2. Fitting noise has to be considered, which shows up since quite fine broadening effects have to be extracted at rather high accuracy in order to be used for pressure determination. This noise (9 hPa (1σ) at 220 hPa) is also a consequence of the very harsh measurement conditions, such as the high gas velocity of up to 900 km h^{-1}, which also causes very fast optical transmission fluctuations. In addition the signal is impeded by fluctuating background radiance impinging on the open detector (see Eq. 1). This background, mainly solar radiation, depends on the angle between the aircraft (cell, mirror, detector) and the sun. In some flight situations the background light amounts from a few to 10 % of the total light entering the detector, in other extreme cases the sunlight contribution is 4 times stronger than the total laser radiation detected. However this is corrected for every single absorption TDLAS signal, i.e. 240 times per second: background light effects can thus be suppressed very effectively in the vast majority of the typical flight situations.

3. Further, one has to consider imperfect separation of the self-broadening effects, owing to the strong (100 times) and fast H_2O concentration fluctuation (see Fig. 8, green line and right-hand scale).

4. Finally, the strong H_2O absorbance variations also lead to strong variations in the SNR and hence to limitations in the fitting process.

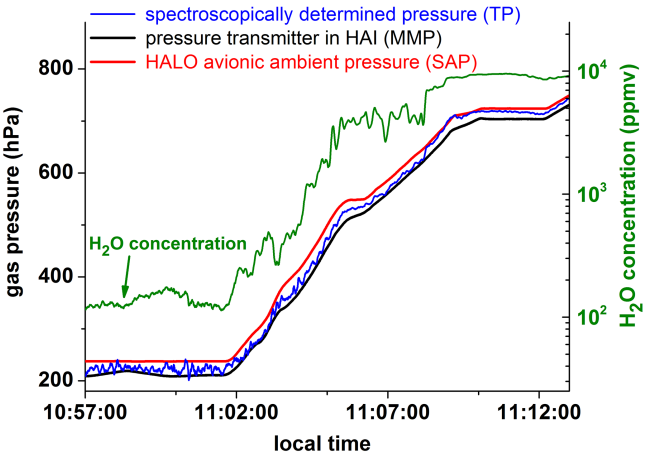

Figure 8. Superposition of all three pressure measurands (bottom traces, left scale) as well as the measured water vapour profile (top trace and right scale) vs. time during an aircraft descent from 200 to 800 hPa. Despite the micro-mechanical HAI pressure transmitter (MMP, black) being placed very close to the open-path measurement volume, clear discrepancies compared to the other pressure sensors are visible. These are attributed to the high-speed flow around the HAI sensor and especially towards the rectangular pressure transmitter interface (see Fig. 6), which can cause complex dynamic effects depending on the HAI orientation in the flow. The red curve shows static ambient pressure measurements (SAP) from HALO's avionic sensors (Giez, 2012), located "in front" of Halo in the nose boom. The typical large atmospheric H_2O concentration variations (log scale) are visible, indicating the necessity for detailed corrections of the optical pressure measurement (explained in detail in text).

Despite these imperfections, Fig. 8 nicely illustrates the mutual validation of all three sensors, as the small differences (averaged difference SAP–MMP $= 28$ hPa, averaged difference SAP–TP $= 13$ hPa; see also Figs. 9 and 10) can be attributed to the different measurement locations and sensor installations.

This result therefore not only justifies water vapour as a suitable target species for optical pressure determination. It also allows the validation of the optical pressure technique permanently – without any additional hardware effort – while the standard evaluation of the HAI water vapour signals is maintained at any given time.

The *disturbed* intercomparison case (shown in Fig. 9) removes the apparent redundancy of the three pressure signals and explains why a "local" pressure measurement at the HAI pylons is needed, for example to recognise fluid-dynamically critical situations, which may lead to significant systematic

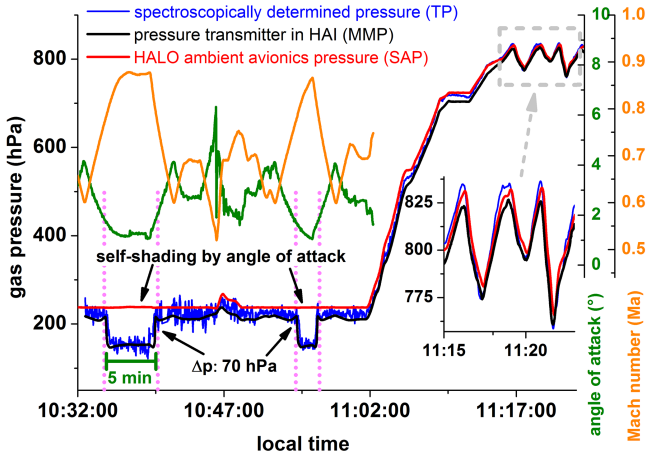

Figure 9. Intercomparison of static ambient avionic pressure (SAP, red), micro-mechanical HAI pressure (MMP, black) and spectroscopic TDLAS pressure (TP, blue) during certain HALO high-altitude flight manoeuvres and a subsequent descent. A clear incidence of HALO's aerodynamic influence of the effective pressure within the open-path volume of HAI, leading to a strong deviation between the SAP and the HAI pressures (MMP/TP), can be seen on the left between 10:30 and 11:00. The block-shaped pressure deviations of 70 hPa (i.e. 30 % relative Δp) are caused by self-shading of HAI during a HALO manoeuvre caused by a change in the angle of attack (green line, right scale in green) and velocity (orange line and scale on right) of the aircraft. (The resulting constraints in using HALO's avionic pressure measurement are discussed in the text.) At lower flight heights and less critical manoeuvres ($t = 11{:}20$), all three pressure signals agree within 1 % (9 hPa at about 830 hPa) (see inset on the right).

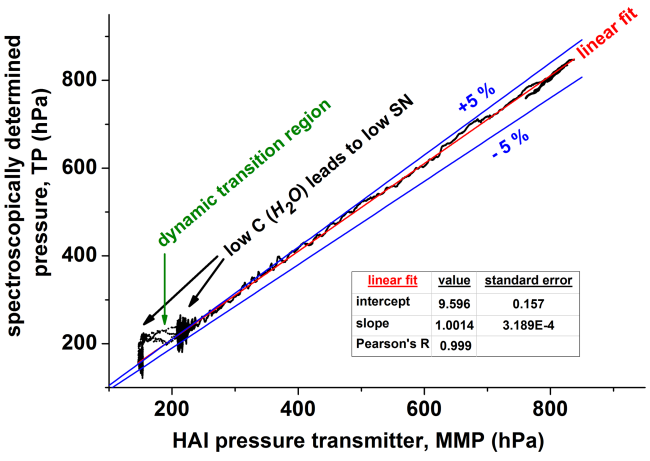

Figure 10. Correlation plot between HAI's micro-mechanical pressure transmitter (MMP) and the spectroscopic TDLAS pressure measurement (TP). Overall, the correlation can be well represented with a linear fit (red line) with a slope of 1.0014 and $R = 0.9992$. The complex flow dynamic effects (e.g. Fig. 8) have some influence on the correlation, particularly at lower pressure, and can lead to self-shading effects (marked green; see Fig. 9) in the dynamic transition region. The higher noise level at low pressures results from the strong H_2O decrease at higher flight heights.

deviations in the pressure as well as the H_2O concentration measurement derived from the HAI open-path cell.

Similar to the figures above, Fig. 9 shows the three measured pressure values in the same colour code. On the right-hand side (at $t > 11{:}02$ LT), a steep descent from 200 to 800 hPa occurs, followed by four fast, repetitive, small-scale, ascent–descent movements with a pressure amplitude of only 50 hPa (see inset Fig. 9 on the right). As in the case of the previous figure, all sensors nicely overlap, with an average deviation over the whole time of only within 1 % (9 hPa at about 830 hPa).

The left-hand side of Fig. 9 ($t = 10{:}32$ to $11{:}02$) shows, in contrast to Fig. 8, on two occasions a significant discrepancy between the SAP and both HAI pressure sensors. These strong, several-minute-long, block-shaped pressure deviations with a relative magnitude of 30 % to SAP ($\Delta p =$ approximately 70 hPa) are not visible by the SAP. However, MMP and TP agree in this situation quite well with regard to the amplitude as well as the phase of this pressure excursion (to better than 5 %). If this deviation were measured by only MMP, it would be very difficult to exclude any malfunction, e.g. due to ice accumulation in front of or in the MMP interface. The excellent match between MMP and TP, however, falsifies this assumption and thus calls for an explanation other than a malfunction of the MMP sensor.

This explanation can be found by looking at additional aircraft parameters which influence the flow field around HALO. Also shown in Fig. 9 are the travelling speed of HALO (i.e. Mach number, orange line and scale on the left) and the angle between the atmospheric fluid velocity vector and the wing surface (i.e. angle of attack, green line and scale). As depicted, the strong pressure excursions correlate in an almost "binary" way with the crossing of a minimum Mach number or a maximum angle of attack (dashed lines).

Obviously the flow around the HAI sensor is obstructed or stalled at a certain angle of attack/speed of the aircraft, and thus the pressure in between the HAI pylons changes abruptly. With a fully detailed model of the flow around the aircraft and its external component parts, these pressure effects could also be simulated and superimposed on the avionic pressure signal. But these calculations would have to be recomputed for every flight parameter set (flight speed, HALO's orientation), thus involving intensive computation over several hours of flight, which makes this a slow and unattractive approach. Therefore, the possibility of validating the pressure transmitter in an open-path cell with the same raw data for final humidity evaluation allows for a much easier clarification and verification of malfunctions (if there are any), thus allowing for easy but advanced data quality management.

Finally (see Fig. 10) we compare the HAI pressure sensors by directly correlating the data from Fig. 9. The pressure

detected by the MMP (the internal pressure transmitter in the open-path cell) and the TP (the spectroscopically determined pressure) show an excellent agreement which falls very close to the 1 : 1 bisector line. A linear fit is made to elucidate the correlation quantitatively and yields a very small slope deviation of only 0.14 % from the ideal bisector slope. This nicely demonstrates the good agreement and the linearity of the two sensors. The correlation of both sensors also falls well within the ±5 % corridor defined by the overall TP sensor uncertainty of 5.1 %. The correlation plot also shows well that most of the individual data points over a wide pressure – and hence H_2O concentration – range match well. Only at quite low pressures, where the SNR dropped significantly, does a weakened correlation, caused by the dynamic changes in the flight pattern at the high flight levels, appear. Figure 10 also clearly shows the transition regions resulting from the pressure drop at the edges as a dynamic effect, and the higher noise level caused by the low water vapour concentration (approximately 150 ppmv; Fig. 8). Even fine details can be found: the offset of 9.5 hPa extracted from the slope fit can be interpreted as a consequence of the air mass movement towards the rectangular pressure transmitter interface, which leads – as mentioned above – to a local pressure reduction. In the future, this offset will be an interesting parameter to be checked when an entire CFD model becomes available. Overall, Figs. 8–10 nicely allow for a mutual validation of the two HAI pressure sensors with each other and during suitable conditions also of the TP and the MMP with the avionic pressure data within a few percent.

5 Conclusion and outlook

Highly accurate pressure measurements on research aircraft are quite difficult to realise because of the complex flow dynamics and their dependency on several other airborne flight parameters. To solve many flight issues, an accurate knowledge of the static ambient pressure is required. Static pressure sensors are typically available with a high level of accuracy. However, the determination of the exact pressure at a specific location on the fuselage of an aircraft requires computationally intensive simulations (using CFD models) for every flight parameter set.

In this paper, we presented an integrated approach to a purely spectroscopic, calibration-free pressure determination using water vapour as the sensor species and HAI as the sensing instrument. The HAI instrument is initially designed for multiphase water vapour detection and serves here as an additional TDLAS-based gas pressure sensor in the light path region of the HAI open-path White cell on the aircraft fuselage. The optical pressure measurement was designed to be calibration-free and is purely based on the knowledge of the relevant spectral parameters of the sensor molecule describing the line broadening. The correction process, which has to be executed to obtain accurate pressure values, has been described and takes self-broadening and temperature dependence of the broadening parameters into account. For the spectroscopic pressure detection using HAI, we determine – despite the high atmospheric water vapour variability – a pressure uncertainty of 3.2 % for laboratory conditions and 5.1 % under flight operating conditions in the field.

The spectroscopic pressure determination was compared in the range of 150–800 hPa with (a) a HAI-internal micro-mechanical pressure sensor and (b) the static ambient pressure measurements of the aircraft avionics. The linearity deviation between MMP and TP was 0.14 %. A small dynamically induced pressure offset of 9.5 hPa was found.

Occasional dynamic deviations from the static ambient avionic pressure confirm the need for permanent CFD simulations under all flight conditions for validating the measured pressure. Alternatively, open-path species sensors like HAI need a well-designed micro-mechanical sensor or, better still, spectroscopic pressure detection.

In the standard evaluation mode of HAI, this pressure detection is used for stabilising and accelerating the fitting process. However, owing to the integrated approach, a pressure validation can be done at any time using the same raw data, implying that it is not a common single pre- or post-validation process but a parallel execution.

The measured pressure data can additionally be included as validation parameters for the development of a larger and more accurate CFD simulation model for inlet systems such as the open-path cell.

For that purpose, the laser-based high-speed optical pressure measurement can be seen as a more general concept which also can be realised using other gas species. CO_2 in particular appears quite useful for dedicated optical pressure sensors as it is much more evenly distributed in the atmosphere, and therefore the pressure measurement could also be realisable, for example, in the UTLS. Due to the low CO_2 concentration (compared to water vapour), self-broadening effects are drastically reduced and also relatively constant during flight level variations, which would simplify the data evaluation significantly and make the optical pressure signal even more robust. The CO_2 2.0 µm and especially the 2.7 µm band are particular attractive for pressure sensing. Assuming 100 hPa outside pressure, 400 ppmv CO_2 in air and a 4 m optical path length, peak absorptions up to 50 % can be expected in the 2.7 µm range (3 % at 2 µm). The 2.7 µm CO_2 lines are even more attractive for pressure sensing and should allow for significantly better pressure resolution than the 9 hPa named above due to the much higher absorption compared to the H_2O lines used in HAI. With regard to performance, the 2.7 µm lasers needed are fully comparable to the 2.6 µm lasers used currently in HAI for water vapour measurements and should also be very easy to integrate due to identical operating conditions and form factors. Therefore, the 2.7 µm CO_2 lines appear as a quite promising, high-resolution extension to the H_2O-based pressure sensing. However, owing to the constantly rising operational and

certification costs for aircraft instrumentation, this has to be combined with the scientific use of the target concentration data and will therefore have to be planned as a contribution in a future campaign.

Acknowledgements. Parts of this work were funded by the Deutsche Forschungsgemeinschaft (DFG) via FKZ EBE 235/3 and SCHI 872/2.

The authors wish to thank M. Krämer (Forschungszentrum Jülich) for her strong, continued support of the project; A. Giez, M. Zöger and V. Dreiling, representatives of the Deutsches Zentrum für Luft- und Raumfahrt Oberpfaffenhohen, for providing the HALO avionic data; and A. Engel and H. Bönisch (Goethe Universität Frankfurt) for their coordination of the TACTS campaign.

Edited by: H. Harder

References

Armstrong, B.: Spectrum line profiles: the Voigt function, J. Quant. Spectrosc. Ra., 7, 61–88, doi:10.1016/0022-4073(67)90057-X, 1967.

Brown, M., Barone, D., Barhorst, T., Eklund, D., Gruber, M., Mathur, T., and Milligan, R.: TDLAS-based measurements of temperature, pressure, and velocity in the isolator of an axisymmetric scramjet, in: 46th AIAA/ASME/SAE/ASEE Joint Propulsion Conference & Exhibit, 6989, doi:10.2514/6.2010-6989, 2010.

Buchholz, B., Afchine, A., Klein, A., Barthel, J., Kallweit, S., Klostermann, T., Krämer, M., Schiller, C., and Ebert, V.: Simultaneous Gas-Phase and Total Water Detection for Airborne Applications with a Multi-Channel TDL Spectrometer at 1.4 µm and 2.6 µm, Geophys. Res. Abstr., 15(EGU2013-7311-3), EGU General Assembly 2013, Vienna, Austria, 2013a.

Buchholz, B., Kühnreich, B., Smit, H. G. J., and Ebert, V.: Validation of an extractive, airborne, compact TDL spectrometer for atmospheric humidity sensing by blind intercomparison, Appl. Phys. B, 110, 249–262, doi:10.1007/s00340-012-5143-1, 2013b.

Buchholz, B., Böse, N., and Ebert, V.: Absolute validation of a diode laser hygrometer via intercomparison with the German national primary water vapor standard, Appl. Phys. B, 116, 883–899, doi:10.1007/s00340-014-5775-4, 2014.

Dicke, R.: The effect of collisions upon the Doppler width of spectral lines, Phys. Rev., 89, 472–473, doi:10.1103/PhysRev.89.472, 1953.

Diskin, G. S., Podolske, J. R., Sachse, G. W., and Slate, T. A.: Open-path airborne tunable diode laser hygrometer, in: Proc. SPIE 4817, Diode Lasers and Applications in Atmospheric Sensing, 4817, 196–204, 2002.

Ebert, V. and Wolfrum, J.: Absorption spectroscopy, in: Optical Measurements – Techniques and Applications (Heat and Mass Transfer), edited by: Mayinger, F. and Feldmann, O., Springer, Heidelberg, München, 273–312, 2000.

Ebert, V., Teichert, H., and Fernholz, T.: In situ measurement of CO, H_2O and gas temperature in a lignite-fired power-plant, Appl. Optics, 42, 2043–2051, doi:10.1364/AO.42.002043, 2003.

Engel, A., Boenisch, H., and TACTS-Team: An overview on the TACTS mission using the new German research aircraft HALO in summer 2012, EGU General Assembly, 15(EGU2013-9191) [online] available at: http://adsabs.harvard.edu/abs/2013EGUGA..15.9191E, last access: 1 August 2013.

Farooq, A., Jeffries, J., and Hanson, R.: In situ combustion measurements of H_2O and temperature near 2.5 µm using tunable diode laser absorption, Measurement Science and Technology, 19, 075604, doi:10.1088/0957-0233/19/7/075604, 2008.

Galatry, L.: Simultaneous effect of Doppler and foreign gas broadening on spectral lines, Phys. Rev., 122, 1218–1223, doi:10.1103/PhysRev.122.1218, 1961.

Giesen, T., Schieder, R., Winnewisser, G., and Yamada, K. M. T.: Precise measurements of pressure broadening and shift for several H_2O lines in the $\nu 2$ band by argon, nitrogen, oxygen, and air, J. Mol. Spectrosc., 153, 406–418, doi:10.1016/0022-2852(92)90485-7, 1992.

Giez, A.: Effective test and calibration of a trailing cone system on the Atmospheric Research aircraft HALO, in: Proceedings of the 56th Annual Symposium of the Society of Experimental Test Pilots, September 2012, 2012.

Heinonen, M.: A comparison of humidity standards at seven European national standards laboratories, Metrologia, 39, 303–308, doi:10.1088/0026-1394/39/3/7, 2002.

Herbert, F.: Spectrum line profiles: a generalized Voigt function including collisional narrowing, J. Quant. Spectrosc. Ra., 14, 943–951, doi:10.1016/0022-4073(74)90021-1, 1974.

Hunsmann, S., Wagner, S., Saathoff, H., Möhler, O., Schurath, U., and Ebert, V.: Messung der Temperaturabhängigkeit der Linienstärken und Druckverbreiterungskoeffizienten von H_2O-Absorptionslinien im 1.4 µm Band, in: VDI Berichte (1959), VDI Verlag, Düsseldorf, 149–164, 2006.

Joint Committee for Guides in Metrology (JCGM): Evaluation of measurement data – Guide to the expression of uncertainty in measurement JCGM 100, 2008, BIPM, available at: www.bipm.org (last access: 30 April 2014), 2008.

Klim, A.: A comparison of methods for the calculation of Voigt profiles, J. Quant. Spectrosc. Ra., 26, 537–545, doi:10.1016/0022-4073(81)90041-8, 1981.

Kochanov, V. P.: Collision line narrowing and mixing of multiplet spectra, J. Quant. Spectrosc. Ra., 66, 313–325, doi:10.1016/S0022-4073(99)00116-8, 2000.

Kochanov, V. P.: Efficient approximations of the Voigt and Rautian–Sobelman profiles, Atmos. Ocean. Optics, 24, 432–435, doi:10.1134/S1024856011050071, 2011.

Krautstrunk, M. and Giez, A.: The transition from FALCON to HALO era airborne atmospheric research, in: Atmospheric Physics: Background – Methods – Trends Research Topics in Aerospace, edited by: Schumann, U., Springer-Verlag Berlin Heidelberg, 609–624, ISBN978-3-642-30182-7, 2012.

Lackner, M.: Tunable diode laser absorption spectroscopy (TDLAS) in the process industries – a review, Rev. Chem. Eng., 23, 65–147, doi:10.1515/REVCE.2007.23.2.65, 2011.

Lepère, M.: Line profile study with tunable diode laser spectrometers, Spectrochim. Acta A, 60, 3249–3258, doi:10.1016/j.saa.2003.12.052, 2004.

May, R. D.: Open-path, near-infrared tunable diode laser spectrometer for atmospheric measurements of H_2O, J. Geophys. Res., 103, 19161–19172, doi:10.1029/98JD01678, 1998.

Mihalcea, R., Baer, D., and Hanson, R.: Diode laser sensor for measurements of CO, CO_2, and CH_4 in combustion flows, Appl. Optics, 36, 8745–8752, doi:10.1364/AO.36.008745, 1997.

Muecke, R. J., Scheumann, B., Slemr, F., and Werle, P. W.: Calibration procedures for tunable diode laser spectrometers, in: Proc. SPIE 2112, Tunable Diode Laser Spectroscopy, Lidar, and DIAL Techniques for Environmental and Industrial Measurement, 2112, 87–98, doi:10.1117/12.177289, 1994.

Olivero, J. and Longbothum, R.: Empirical fits to the Voigt line width: a brief review, J. Quant. Spectrosc. Ra., 17, 233–236, doi:10.1016/0022-4073(77)90161-3, 1977.

Ortwein, P., Woiwode, W., Wagner, S., Gisi, M., and Ebert, V.: Laser-based measurements of line strength, self-and pressure-broadening coefficients of the $H^{35}ClR$ (3) absorption line in the first overtone region for pressures up to 1 MPa, Appl. Phys. B, 100, 341–347, doi:10.1007/s00340-009-3862-8, 2010.

Peach, G.: Theory of the pressure broadening and shift of spectral lines, Adv. Phys., 30, 367–474, doi:10.1080/00018738100101467, 1981.

Pickett, H. M.: Effects of velocity averaging on the shapes of absorption lines, J. Chem. Phys., 73, 6090, doi:10.1063/1.440145, 1980.

Pogány, A., Mohácsi, Á., Jones, S. K., Nemitz, E., Varga, A., Bozóki, Z., Galbács, Z., Weidinger, T., Horváth, L., and Szabó, G.: Evaluation of a diode laser based photoacoustic instrument combined with preconcentration sampling for measuring surface–atmosphere exchange of ammonia with the aerodynamic gradient method, Atmos. Environ., 44, 1490–1496, doi:10.1016/j.atmosenv.2010.01.038, 2010.

Pustogov, V. V., Kuhnemann, F., Sumpf, B., Heiner, Y., and Herr, K.: Pressure broadening of NO_2 by NO_2, N_2, He, Ar, and Kr studied with TDLAS, J. Mol. Spectr., 167, 288–299, doi:10.1006/jmsp.1994.1236, 1994.

Rautian, S. and Sobel'man, I.: The effect of collisions on the Doppler broadening of spectral lines, Sov. Phys. Usp., 9, 209–236, doi:10.1070/PU1967v009n05ABEH003212, 1967.

Rothman, L. S., Gordon, I. E., Barbe, A., Benner, D. C., Bernath, P. F., Birk, M., Boudon, V., Brown, L. R., Campargue, A., and Champion, J.-P.: The HITRAN 2008 molecular spectroscopic database, J. Quant. Spectrosc. Ra., 110, 533–572, doi:10.1016/j.jqsrt.2009.02.013, 2009.

Schiff, H. I., Mackay, G. I., and Bechara, J.: The use of tunable diode laser absorption spectroscopy for atmospheric measurements, Res. Chem. Intermediat., 20, 525–556, doi:10.1163/156856794X00441, 1994.

Schlager, H.: ESMval (Earth System Model Validation), available at: http://www.pa.op.dlr.de/ESMVal (last access: 30 April 2014), 2014.

Schlosser, H. E., Fernholz, T., Teichert, H., and Ebert, V.: In situ detection of potassium atoms in high-temperature coal-combustion systems using near-infrared-diode lasers, Spectrochim. Acta A, 58, 2347–2359, doi:10.1016/S1386-1425(02)00049-5, 2002.

Schulz, C., Dreizler, A., Ebert, V., and Wolfrum, J.: Combustion diagnostics, in: Handbook of Experimental Fluid Mechanics, edited by: Tropea, C., Yarin, A. L., and Foss, J. F., Springer, Berlin, Heidelberg, 1241–1316, 2007.

Teichert, H.: Entwicklung und Einsatz von Diodenlaser-Spektrometern zur simultanen In-situ-Detektion von CO, O_2 und H_2O in technischen Verbrennungsprozessen, Ph.D., Ruprecht-Karls Universität Heidelberg [online], available at: http://archiv.ub.uni-heidelberg.de/volltextserver/3612/ (last access: 6 February 2014), 2003.

Varghese, P. L. and Hanson, R. K.: Collisional narrowing effects on spectral line shapes measured at high resolution, Appl. Optics, 23, 2376–2385, doi:10.1364/AO.23.002376, 1984.

Vorsa, V., Dheandhanoo, S., Ketkar, S. N., and Hodges, J. T.: Quantitative absorption spectroscopy of residual water vapor in high-purity gases: pressure broadening of the 1.39253-microm H_2O transition by N_2, HCl, HBr, Cl_2, and O_2, Appl. Optics, 44, 611–619, doi:10.1364/AO.44.000611, 2005.

Werle, P.: A review of recent advances in semiconductor laser based gas monitors, Spectrochim. Acta A, 54, 197–236, doi:10.1016/S1386-1425(97)00227-8, 1998.

White, J.: Very long optical paths in air, J. Opt. Soc. Am., 66, 411–416, doi:10.1364/JOSA.66.000411, 1976.

Yang, H., Greszik, D., Wlokas, I., Dreier, T., and Schulz, C.: Tunable diode laser absorption sensor for the simultaneous measurement of water film thickness, liquid- and vapor-phase temperature, Appl. Phys. B, 104, 21–27, doi:10.1007/s00340-011-4643-8, 2011.

Zondlo, M., Paige, M. E., Massick, S. M., and Silver, J.: Vertical cavity laser hygrometer for the national science foundation Gulfstream-V aircraft, J. Geophys. Res., 115, 20309, doi:10.1029/2010JD014445, 2010.